Hindawi Publishing Corporation
The Scientific World Journal
Volume 2014, Article ID 349457, 7 pages
http://dx.doi.org/10.1155/2014/349457

Research Article

Microwave Synthesis, Characterization, and Photoluminescence Properties of Nanocrystalline Zirconia

A. K. Singh[1] and Umesh T. Nakate[2]

[1] *DRDO Center for Piezoceramics and Devices, ARDE, Pashan, Pune 411021, India*
[2] *Nanomaterials and Sensors Laboratory, Defence Institute of Advanced Technology (DU), Girinagar, Pune 411025, India*

Correspondence should be addressed to A. K. Singh; draksingh@hotmail.com

Received 30 August 2013; Accepted 24 October 2013; Published 21 January 2014

Academic Editors: P. Li, E. Poirier, and H. Yahiro

We report synthesis of ZrO_2 nanoparticles (NPs) using microwave assisted chemical method at 80°C temperature. Synthesized ZrO_2 NPs were calcinated at 400°C under air atmosphere and characterized using FTIR, XRD, SEM, TEM, BET, and EDS for their formation, structure, morphology, size, and elemental composition. XRD results revealed the formation of mixed phase monoclinic and tetragonal ZrO_2 phases having crystallite size of the order 8.8 nm from most intense XRD peak as obtained using Scherrer formula. Electron microscope analysis shows that the NPs were less than 10 nm and highly uniform in size having spherical morphology. BET surface area of ZrO_2 NPs was found to be 65.85 m^2/g with corresponding particle size of 16 nm. The band gap of synthesized NPs was found to be 2.49 eV and PL spectra of ZrO_2 synthesized NPs showed strong peak at 414 nm, which corresponds to near band edge emission (UV emission) and a relatively weak peak at 475 and 562 nm.

1. Introduction

ZrO_2 (zirconia) is a material of great technological importance, having good natural color, high strength, high toughness, high chemical stability, excellent corrosion, and chemical and microbial resistance [1, 2]. ZrO_2 is a wide band gap P-type semiconductor that exhibits abundant oxygen vacancies on its surface. The high ion exchange capacity and redox activities make it useful in many catalytic processes as a catalyst [3]. ZrO_2 is also an important dielectric material that is being investigated for potential application as an insulator in transistors in future nanoelectric devices [4]. Garcia et al. [5] have highlighted its potential to replace SiO_2 in advanced metal oxide semiconductor (MOS) devices and in optical applications.

ZrO_2 has three well-defined crystal structures/phases, that is, cubic (c-ZrO_2), tetragonal (t-ZrO_2), and monoclinic (m-ZrO_2), under normal atmosphere and at different temperatures [6, 7]. Generally, m-ZrO_2 phase is thermodynamically stable up to 1100°C, t-ZrO_2 phase exists in the temperature range of 1100–2370°C, and the cubic phase is found above 2370°C [8]. There are contradictory reports on the existence of various phases under different conditions of temperatures. Recently, existence of t-ZrO_2 at low temperature has been reported by many researchers [9–11]. Ciuparu et al. [9] have reported the initial existence of amorphous phase, and after heating above 750°C, t-phase formation has been observed, and transition from tetragonal to monoclinic has been observed after calcinations at 1200°C. Shukla et al. [11] have observed nucleation of t-ZrO_2 phase from the amorphous phase at 400°C, which becomes stable at 600°C, and after calcination at 800°C complete tetragonal-to-monoclinic phase transformation has been reported.

ZrO_2 has many interesting characteristics, such as superior mechanical characteristics, increased fracture toughness, hardness, strength, high thermal expansion coefficient, low thermal conductivity, superplastic deformation, phase stability, and good chemical resistance, which have resulted in a variety of industrial and engineering applications that include high durability coating, catalytic agents, medical prosthetics, cutting tools, synthetic jewels, high density grinding media, wear components, bearings, seals, valves, nose cones and

tiles for space shuttles and missiles, turbines, and the most demanding aviation engines [12–17]. It also has the best performance as ceramic dental material. ZrO_2 has found uses in solid oxide fuel cells [18] and in NO_x, O_2 gas sensors [19]. The fully stabilized ZrO_2 is also well suited for high temperature energy conversion systems, due to its high oxygen ion transport capabilities and good long-term stability.

In spite of many unique characteristics, it has serious drawback for engineering application because it undergoes phase transformation with a change in volume at high temperatures, whereas, for optical and electronic applications, precise evaluation of its band gap is of significance since wide variation has been reported in its band gap [5, 9]. ZrO_2 is usually in the form of m-ZrO_2 at room temperature. Thus, the synthesis and room temperature stabilization methods of nano-t-ZrO_2 are very important and of scientific significance with application prospects.

To prepare nano-ZrO_2, several methods have been reported that include sol-gel, flame spray, combustion, glycothermal process, hydrothermal processing, and precipitation routes [7, 20–24]. In particular, a chemical solution method, which involves formation of a stable particle by a direct reaction between the atoms or reaction species, provides the most suitable way of synthesizing a sample of imperfection/defect free particles. The sol-gel method is one of the most common methods that have been used to synthesize nano-ZrO_2. Many of these methods of nano-ZrO_2 preparation use a synthetic template material, which is not economical and relatively more expensive. In the literature, there are few reports on the usage of microwave method for the synthesis of ZrO_2 [10, 25, 26] which is the novel route of synthesis of metal oxide NPs, being clean, cost-effective, energy efficient, eco-friendly, rapid and convenient method of heating, and results in higher yields in shorter reaction times [27]. Here, we report simple, low temperatures of synthesis of nanocrystalline ZrO_2 NPs using microwave assisted method. To the best of our knowledge, the reaction temperature we used is the lowest used in the synthesis of ZrO_2 NPs. The synthesized NPs of ZrO_2 were investigated using FTIR, XRD, SEM-EDS, and TEM analysis.

2. Experimental Details

2.1. Synthesis. All chemicals used in the synthesis have been used as received from chemical suppliers without any further purification and processing. 50 mL of 0.1 M zirconium oxychloride octahydrate solution was prepared and 15 mL 1 N NaOH solution was added dropwise in given solution with continuous stirring, after precipitation precursor solution was kept in microwave oven for 12 min with power 420 W and temperature 80°C using RAGA'S microwave system. Microwave used for this experiment was of power range of 140 W to 700 W. Obtained precipitate was filtered, washed 2-3 times with DI water (18.2 MΩ·cm resistivity) and then dried at temperature 150°C for several hours. Dried powder was crushed and calcinated in air atmosphere at 400°C for 2 hours and obtained sample was characterized.

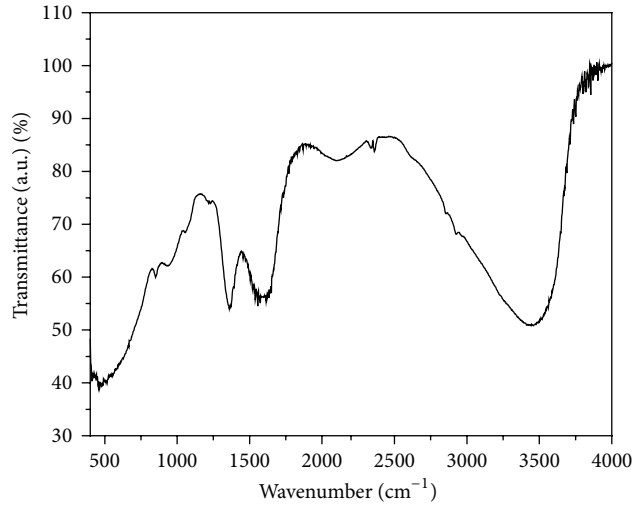

FIGURE 1: FTIR spectra of ZrO_2 of NPs in the 400–4000 cm^{-1} region.

2.2. Characterization. The prepared annealed samples were characterized for their formation, structure, morphology, and elemental composition using Fourier transform infrared (FTIR) spectroscopy, X-ray diffraction analysis (XRD), scanning electron micrograph (SEM), transmission electron micrograph (TEM), energy dispersive spectrometer (EDS), Brunauer, Emmett and Teller (BET), and UV-Vis spectroscopy. FTIR of samples was performed using Shimadzu Affinity-1 FTIR spectrometer. Crystallographic study was carried out using Bruker AXS, Germany (Model D8 Advanced), diffractometer in the scanning range of 20–80° (2θ) using Cu Kα radiations of wavelength 1.5406 Å. JEOL ASM 6360A scanning electron microscope (SEM) was used to study the morphology and the elemental analysis. Transmission electron microscopy (TEM) of samples was carried out using FEI-Tecnai $G^2$20. Measurement of BET surface area was carried out for nitrogen adsorption using a Micromeritics Ins., USA. UV-Vis spectroscopy of samples was done in the range of about 200–800 nm with the help of Ocean Optics HR4000 high-resolution spectrometer. Room temperature photoluminescence properties of NPs were studied using Perkin Elmer LS55 Luminescence Spectrometer in spectral range of 300–800 nm in the wavelength range of 270–320 nm as excitation source.

3. Results and Discussion

3.1. FTIR Analysis. In order to ascertain the molecular nature of the synthesized material, the FTIR spectrum of the ZrO_2 sample was taken as shown in Figure 1. The spectrum of ZrO_2 depends on the nature of the material, preparative procedures used, solid-state structure, and so forth. The observed strong FTIR absorption peak at about 470 cm^{-1} region is due to the Zr–O vibration, which confirm the formation of ZrO_2 structure [28], prominent peak of 1380 cm^{-1} region corresponds to O–H bonding, peak in the region of 1553 cm^{-1} may be due to the adsorbed moisture and in the 3425–3495 cm^{-1} region is attributed to stretching of O–H groups, characteristic of a highly hydrated compound [28].

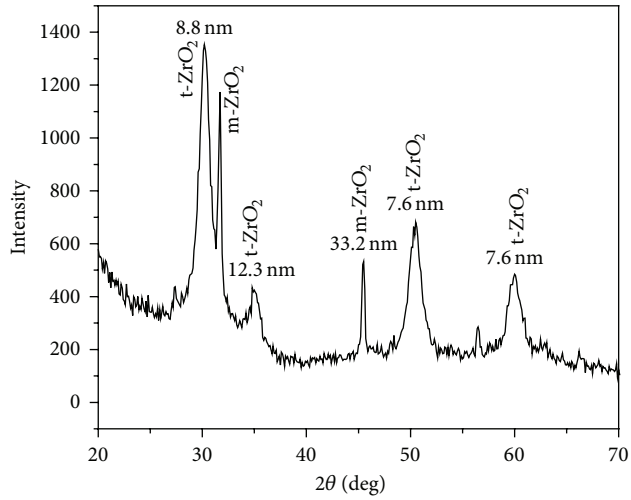

Figure 2: XRD pattern of ZrO_2 NPs calcinated at 400°C.

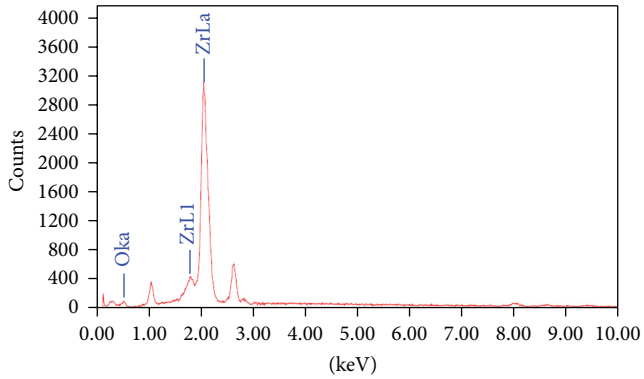

Figure 3: EDAX spectra of ZrO_2 of NPs calcinated at 400°C.

3.2. Crystallographic Analysis. To confirm the phase formation of ZrO_2, XRD pattern of the sample was recorded after calcination in air atmosphere and is shown in Figure 2. The narrow line widths indicate high crystalline nature of the synthesized material. As reported by Shukla et al., [29] scan range of 27–32 degrees contained the strongest lines for monoclinic as well as tetragonal phases. Observed XRD peaks (Figure 2) for sample calcinated at 400°C indicate the formation of t-ZrO_2 and m-ZrO_2 mixed phases. Selection of calcination of sample at 400°C was based on earlier reports indicating that, in order to crystallize ZrO_2, OH ion must be removed under thermal treatment and ZrO_2 is crystallized at a temperature of about 400°C [23]. The distinguishing characteristic peaks for tetragonal occur at $2\theta = 30.2$, 34.5, 50.2, and 60.2 corresponding to the (101), (110), (200), and (211) reflections [JCPDS No. 70-1769] [30, 31]. Stabilization of t-phase at lower temperature is most likely due to low surface energy of the t-phase relative to m-phase. At 300°C, zirconia has an amorphous structure and pure ZrO_2 is crystallized at a temperature of about 400°C [23], but in our case we have observed mixed phase formation.

Mixed phase formation of ZrO_2 is a common feature in zirconia synthesis and has been reported by many

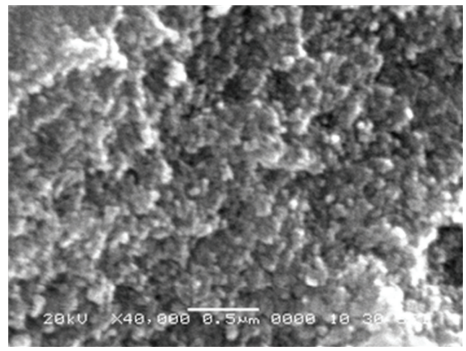

Figure 4: SEM micrographs of ZrO_2 NPs.

authors [28]. Tyagi et al. [23] have reported t-ZrO_2 phase formation at 400°C, and with increase in calcinations temperature they have reported m and t-ZrO_2. The occurrence of metastable tetragonal phase is attributed to the critical crystallite size effect as reported by Garvie [32]. Garvie experimentally showed the existence of a critical size of ~ 30 nm, below which the metastable t-phase is stable and above which the m-phase is stable.

The crystallite size of NPs has been calculated by XRD line broadening of peak using Scherrer's formula [33]

$$D = \frac{K\lambda}{\beta \operatorname{Cos} \theta}, \quad (1)$$

where K is 0.9, λ is wave length of X-ray source (0.1540598 nm), β is full width at half maximum in radians, and θ is Bragg's diffraction angle. Crystallite sizes, calculated using Scherrer's formula (1), are indicated in Figure 2 corresponding to each peak and are the order of 8.8 nm from most intense XRD peak, whereas average size is about 14 nm which is in close agreement with the particle size of ZrO_2 as obtained from BET surface area analysis as discussed.

3.3. Elemental and Morphological Analysis. The synthesis of ZrO_2 NPs was confirmed by recording EDAX spectra and is depicted in Figure 3. Emission peaks, such as OKa, ZrL1, and ZrLa were observed in the EDAX spectrum confirmed the stoichiometry of synthesized NPs. It shows that Zr and O elements are present almost in stiochoimetric ratio.

Morphological investigations of 400°C air calcinated ZrO_2 sample were carried out using SEM and TEM and are shown in Figures 4 and 5, respectively. The morphological characterization highlighted the importance of nanocrystalline ZrO_2 preparation in maintaining the nanostructured phase. It is clear from Figure 4 that NPs are of uniform size. Observation of Figure 4 shows that ZrO_2 particles are spherical in nature and size of the particles is in the nm regime, but size could not be finely resolved from SEM. For the purpose, TEM of sample has been shown in Figure 5. As can be seen from TEM micrographs of sample, some agglomeration has been observed due to different t- and m-phases present in the sample. In spite of agglomeration of the NPs, it can be observed that the sizes of the particles are

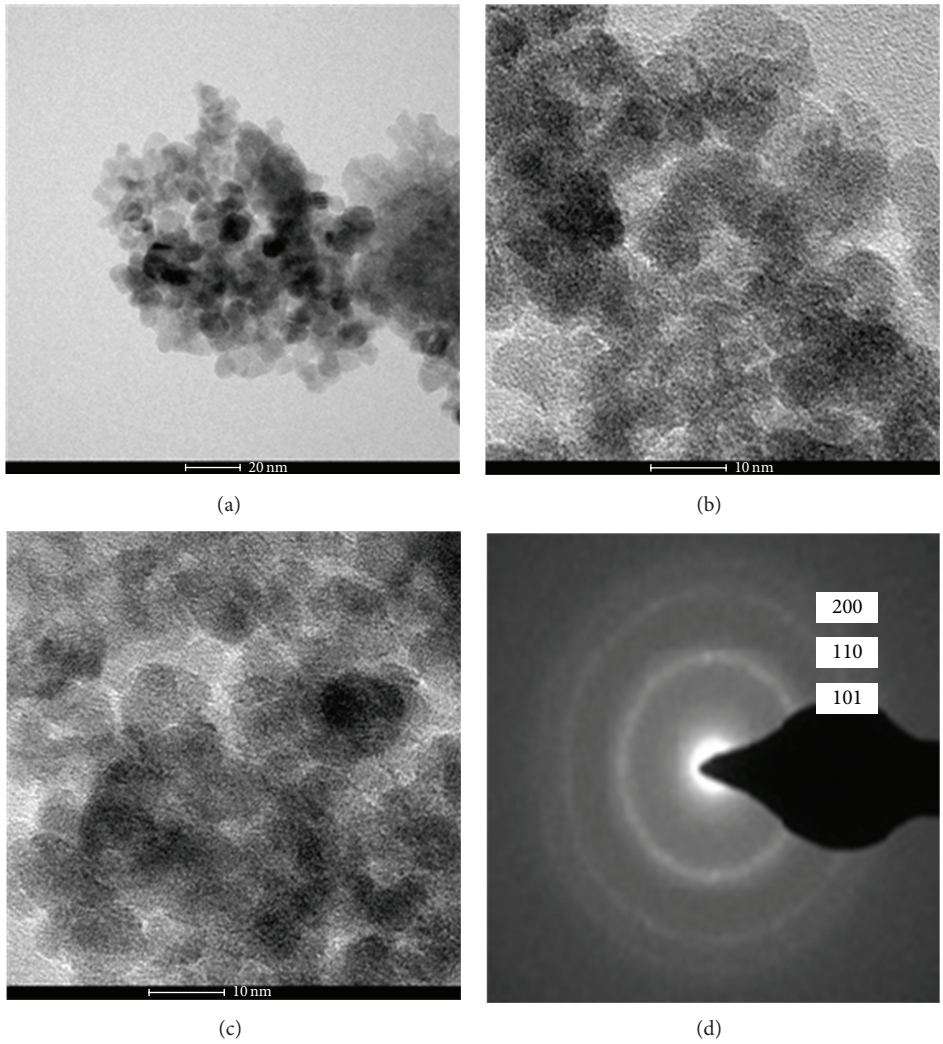

Figure 5: TEM micrographs of ZrO_2 NPs at different magnifications (a)–(c) and electron diffraction pattern taken on a selected area of the sample (d).

of the order 10 nm. The TEM results are also supporting the results of other analyses based on XRD and BET surface area calculations.

Figure 5(d) shows an electron diffraction pattern indicating well-defined quasicontinuous diffraction rings of the sample that calcined at 400°C for 2 h. It is noticeable that the (101), (110), and (200) planes are clearly distinguished [34] as observed in XRD patterns.

3.4. BET Analysis. Surface area analysis was done by nitrogen absorption using BET surface analyzer. NPs size has been calculated from surface area assuming NPs to be of spherical shape, using the following equation [35]:

$$d = \frac{6}{\rho S_{\mathrm{BET}}}, \tag{2}$$

where ρ is the density of ZrO_2 particles and S_{BET} is the BET surface area for powder sample calcinated at 400°C; measured BET surface area has been found to be 65.85 m^2/g. Particle size of ZrO_2 NPs was found to be 16 nm from (2) which is in agreement with the above discussion under the assumption used in the analysis.

3.5. Band Gap Analysis. Reduction in the nanoparticle size can cause change in the optical band gap of metal oxides through the narrowing of the valence and conduction bands [5]. The other important factors that can affect optical band gap are defect centers, mechanical stress, and changes in the crystallinity. Optical absorption spectra of NPs, as shown in Figure 6, have been studied without taking into account the reflection and transmission losses. Tauc's relation of the absorption coefficient (α) with the photon energy ($h\nu$) has been used to determine the band gap energy of sample and is given by

$$\alpha = \frac{\alpha_0 \left(h\nu - E_g\right)}{h\nu}, \tag{3}$$

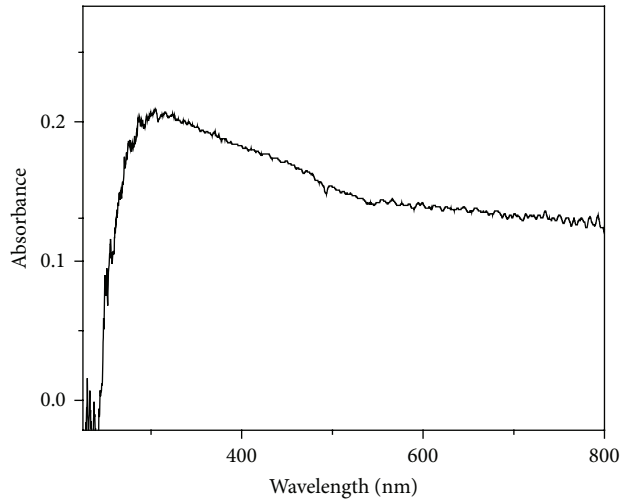

Figure 6: UV-Vis absorbance spectra of microwave synthesized ZrO_2 sample calcinated at 400°C.

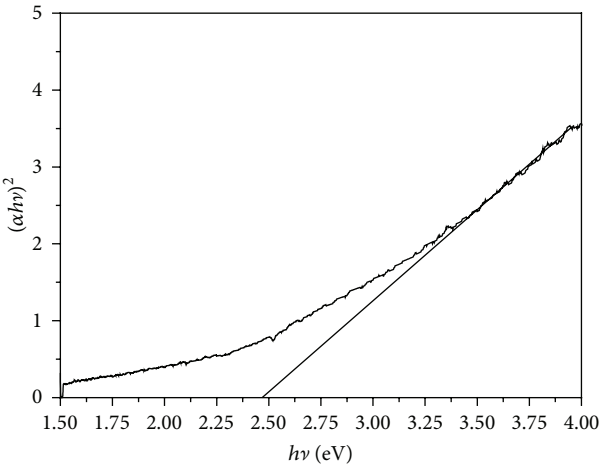

Figure 7: Plot of $(\alpha h\nu)^2$ versus $h\nu$ for ZrO_2 sample calcinated at 400°C.

where α is the absorption coefficient, α_0 is the constant, $h\nu$ is the photon energy, and E_g is the band gap energy of the material. The value of n depends on the probability of transition; it takes values as 1/2, 3/2, 2, and 3 for direct allowed, direct forbidden, indirect allowed, and indirect forbidden, respectively. The variation of $(\alpha h\nu)^2$ versus $h\nu$ is linear at the absorption edge which confirms that ZrO_2 is semiconductor with direct band gap. The plot of $(\alpha h\nu)^2$ versus $h\nu$ is shown in Figure 7. Extrapolating the straight-line portion from higher absorption region of the plot $(\alpha h\nu)^2$ versus $h\nu$ to photon energy axis for zero absorption coefficient value gives the E_g (Figure 8), giving a value of about 2.49 eV [36]. In the literature, a wide variation has been reported in the band gap of ZrO_2 which can be attributed to presence of the zirconia phase, defect state, and morphology.

3.6. Photoluminescence. Photoluminescence (PL) technique is suitable to determine the crystalline quality and presence

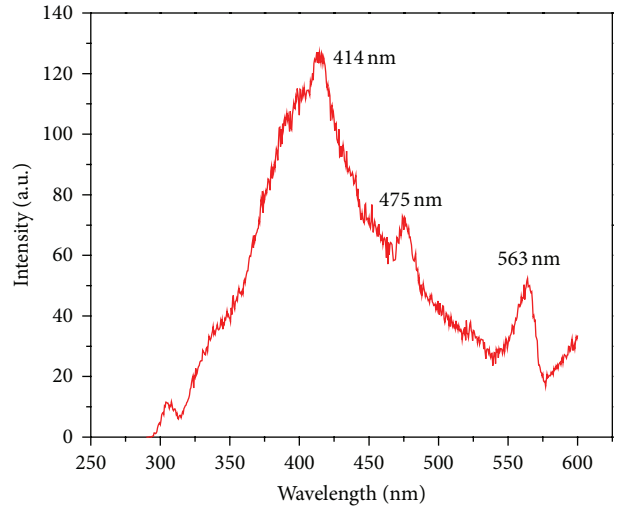

Figure 8: PL spectra of microwave synthesized ZrO_2 sample excited at wavelength 270 nm.

of impurities in the materials, as well as exciton fine structure. Figure 8 shows the room temperature photoluminescence spectra of ZrO_2 NPs excited at four different wavelengths, that is, 270, 290, 300, and 320 nm. Representative fluorescence spectrum with an excitation wavelength of 270 nm shown in Figure 8 exhibited three emission PL bands at around 414, 475, and 563 nm, with 414 nm being the prominent peak. Liang et al. [10] have also reported similar results for t-ZrO_2. As the fluorescence intensity somewhat varied with the excitation wavelength, the fluorescence band position and the band shape stayed nearly the same for these excitation wavelengths. This indicated that the fluorescence involved the same initial and final states in the excitation wavelengths ranging from 270 to 320 nm. It can be accounted for by fast relaxation from the final state arrived at by photo-excitation to those states from which the fluorescence started [37]. The spectrum features a broad fluorescence band cantered at 414 nm. Although the detailed PL mechanism for the nano-ZrO_2 is still under research, we could ascribe the emissions that appear at short wavelength excitation to the near band-edge transitions. The PL peak at 414 nm is attributed to Zr vacancies which is one of the intense peaks considered to be due of band edge emission due to the free-exciton recombination [38]. In the case of the emission at 475 and 563 nm, it should be due to the involvement of mid-gap trap states, such as surface defects and oxygen vacancies. The weak green emission also implies that there are surface defects in ZrO_2 NPs. Large amounts of surface defects exist on the as-synthesized nano-ZrO_2 particles because of their high surface area. The broad band and the substantial red shift of the band maximum compared to the band gap of the bulk material (5.6 eV) strongly indicate that the fluorescence involves extrinsic states. Because the particle size distribution is very narrow, the broad fluorescence band seems to be mostly caused by the small particle size leading to an inhomogeneous broadening from a distribution of surface or defect states.

4. Conclusions

ZrO_2 NPs have been synthesized with the help of a simple microwave assisted chemical process at low temperature. The TEM analysis reveals that the size of the spherical NPs is in the range of 8–10 nm. All analyses have consistently shown fairly uniform NPs with superfine size having mixed t-ZrO_2 and m-ZrO_2 phases. Band gap and PL of the synthesized sample were investigated and band gap of the synthesized ZrO_2 sample was found to be 2.48 eV from Tauc's relation from UV-Vis absorption spectroscopy. Room temperature PL study of synthesized sample showed three emission PL bands at around 414, 475, and 563 nm, with 414 nm being the prominent peak when excited at 270 nm.

Conflict of Interests

The authors declare that they have no conflict of interests regarding the publication of this paper.

Acknowledgments

The authors are thankful to Vice Chancellor, Defence Institute of Advanced Technology, Girinagar, Pune, India, and Director, ARDE, Pune, India for granting permission to publish this work. They are also thankful to Department of Physics, University of Pune, Pune, India, for TEM, SEM, EDS, and XRD of samples.

References

[1] A. Hirvonen, R. Nowak, Y. Yamamoto, T. Sekino, and K. Niihara, "Fabrication, structure, mechanical and thermal properties of zirconia-based ceramic nanocomposites," *Journal of the European Ceramic Society*, vol. 26, no. 8, pp. 1497–1505, 2006.

[2] J. C. Ray, D. Park, and W. Ahn, "Chemical synthesis of stabilized nanocrystaline zirconia powders," *Journal of Industrial and Engineering Chemistry*, vol. 12, no. 1, pp. 142–148, 2006.

[3] J. L. Gole, S. M. Prokes, J. D. Stout, O. J. Glembocki, and R. Yang, "Unique properties of selectively formed zirconia nanostructures," *Advanced Materials*, vol. 18, no. 5, pp. 664–667, 2006.

[4] G. Dutta, K. P. S. S. Hembram, G. M. Rao, and U. V. Waghmare, "Effects of O vacancies and C doping on dielectric properties of ZrO_2: a first-principles study," *Applied Physics Letters*, vol. 89, no. 20, Article ID 202904, 2006.

[5] J. C. Garcia, L. M. R. Scolfaro, A. T. Lino et al., "Structural, electronic, and optical properties of ZrO_2 from ab initio calculations," *Journal of Applied Physics*, vol. 100, no. 10, Article ID 104103, 2006.

[6] D. He, Y. Ding, H. Luo, and C. Li, "Effects of zirconia phase on the synthesis of higher alcohols over zirconia and modified zirconia," *Journal of Molecular Catalysis A*, vol. 208, no. 1-2, pp. 267–271, 2004.

[7] S. Roy, "Nanocrystalline undoped tetragonal and cubic zirconia synthesized using poly-acrylamide as gel and matrix," *Journal of Sol-Gel Science and Technology*, vol. 44, no. 3, pp. 227–233, 2007.

[8] T. Chraska, A. H. King, and C. C. Berndt, "On the size-dependent phase transformation in nanoparticulate zirconia," *Materials Science and Engineering A*, vol. 286, no. 1, pp. 169–178, 2000.

[9] D. Ciuparu, A. Ensuque, G. Shafeev, and F. Bozon-Verduraz, "Synthesis and apparent bandgap of nanophase zirconia," *Journal of Materials Science Letters*, vol. 19, no. 11, pp. 931–933, 2000.

[10] J. Liang, Z. Deng, X. Jiang, F. Li, and Y. Li, "Photoluminescence of tetragonal ZrO_2 nanoparticles synthesized by microwave irradiation," *Inorganic Chemistry*, vol. 41, no. 14, pp. 3602–3604, 2002.

[11] S. Shukla, S. Seal, R. Vij, S. Bandyopadhyay, and Z. Rahman, "Effect of nanocrystallite morphology on the metastable tetragonal phase stabilization in zirconia," *Nano Letters*, vol. 2, no. 9, pp. 989–993, 2002.

[12] Q. Zhang, J. Shen, J. Wang, G. Wu, and L. Chen, "Sol-gel derived ZrO_2-SiO_2 highly reflective coatings," *International Journal of Inorganic Materials*, vol. 2, no. 4, pp. 319–323, 2000.

[13] P. K. Wright and A. G. Evans, "Mechanisms governing the performance of thermal barrier coating," *Current Opinion in Solid State and Materials Science*, vol. 4, pp. 25–30, 1999.

[14] C. Piconi and G. Maccauro, "Zirconia as a ceramic biomaterial," *Biomaterials*, vol. 20, no. 1, pp. 1–25, 1999.

[15] P. Salas, E. de la Rosa-Cruz, L. A. Diaz-Torres, V. M. Castaño, R. Meléndrez, and M. Barboza-Flores, "Monoclinic ZrO_2 as a broad spectral response thermoluminescence UV dosemeter," *Radiation Measurements*, vol. 37, no. 2, pp. 187–190, 2003.

[16] L. Kumari, G. H. Du, W. Z. Li, R. S. Vennila, S. K. Saxena, and D. Z. Wang, "Synthesis, microstructure and optical characterization of zirconium oxide nanostructures," *Ceramics International*, vol. 35, no. 6, pp. 2401–2408, 2009.

[17] J. Karch, R. Birringer, and H. Gleiter, "Ceramics ductile at low temperature," *Nature*, vol. 330, no. 6148, pp. 556–558, 1987.

[18] S. Park, J. M. Vohs, and R. J. Gorte, "Direct oxidation of hydrocarbons in a solid-oxide fuel cell," *Nature*, vol. 404, no. 6775, pp. 265–267, 2000.

[19] E. C. Subbarao and H. S. Maiti, "Science and technology of zirconia," *Advances in Ceramics*, vol. 24, pp. 731–737, 1988.

[20] A. I. Y. Tok, F. Y. C. Boey, S. W. Du, and B. K. Wong, "Flame spray synthesis of ZrO_2 nano-particles using liquid precursors," *Materials Science and Engineering B*, vol. 130, no. 1-3, pp. 114–119, 2006.

[21] S. Shukla, S. Seal, R. Vij, and S. Bandyopadhyay, "Effect of HPC and water concentration on the evolution of size, aggregation and crystallization of sol-gel nano zirconia," *Journal of Nanoparticle Research*, vol. 4, no. 6, pp. 553–559, 2002.

[22] T. K. G. Lam, A. Opalinska, T. Chudoba et al., "Preparation and characterization of ZrO_2:Er^{3+}, Yb^{3+} nanoparticles using a high pressure assisted soft template," *Advances in Natural Sciences: Nanoscience and Nanotechnology*, vol. 1, no. 2, Article ID 025008, 5 pages, 2010.

[23] B. Tyagi, K. Sidhpuria, B. Shaik, and R. V. Jasra, "Synthesis of nanocrystalline zirconia using sol-gel and precipitation techniques," *Industrial and Engineering Chemistry Research*, vol. 45, no. 25, pp. 8643–8650, 2006.

[24] J. S. Kim, D. H. Lee, S. Kang, D. S. Bae, H. Y. Park, and M. K. Na, "Synthesis and microstructure of zirconia nanopowders by glycothermal processing," *Transactions of Nonferrous Metals Society of China*, vol. 19, no. 1, pp. s88–s91, 2009.

[25] K. P. S. S. Hembram and G. M. Rao, "Microwave synthesis of zirconia nanoparticles," *Journal of Nanoscience and Nanotechnology*, vol. 8, no. 8, pp. 4159–4162, 2008.

[26] R. Dwivedi, A. Maurya, A. Verma, R. Prasad, and K. S. Bartwal, "Microwave assisted sol-gel synthesis of tetragonal zirconia nanoparticles," *Journal of Alloys and Compounds*, vol. 509, no. 24, pp. 6848–6851, 2011.

[27] A. K. Singh and U. T. Nakate, "Photocatalytic properties of microwave-synthesized TiO_2 and ZnO nanoparticles using malachite green dye," *Journal of Nanoparticles*, vol. 2013, Article ID 310809, 7 pages, 2013.

[28] L. A. Pérez-Maqueda and E. Matijević, "Preparation and characterization of nanosized zirconium (hydrous) oxide particles," *Journal of Materials Research*, vol. 12, no. 12, pp. 3286–3292, 1997.

[29] S. Shukla, S. Seal, and R. Vanfleet, "Sol-gel synthesis and phase evolution behavior of sterically stabilized nanocrystalline zirconia," *Journal of Sol-Gel Science and Technology*, vol. 27, no. 2, pp. 119–136, 2003.

[30] F. Heshmatpour and R. B. Aghakhanpour, "Synthesis and characterization of superfine pure tetragonal nanocrystalline sulfated zirconia powder by a non-alkoxide sol-gel route," *Advanced Powder Technology*, vol. 23, no. 1, pp. 80–87, 2012.

[31] X. Xu and X. Wang, "Fine tuning of the sizes and phases of ZrO_2 nanocrystals," *Nano Research*, vol. 2, no. 11, pp. 891–902, 2009.

[32] R. C. Garvie, "The occurrence of metastable tetragonal zirconia as a crystallite size effect," *Journal of Physical Chemistry*, vol. 69, no. 4, pp. 1238–1243, 1965.

[33] A. K. Singh, "Synthesis, characterization, electrical and sensing properties of ZnO nanoparticles," *Advanced Powder Technology*, vol. 21, no. 6, pp. 609–613, 2010.

[34] F. Kazemi, A. Saberi, S. Malek-Ahmadi, S. Sohrabi, H. R. Rezaie, and M. Tahriri, "A novel method for synthesis of metastable tetragonal zirconia nanopowders at low temperatures," *Ceramics—Silikáty*, vol. 55, no. 1, pp. 26–30, 2011.

[35] J. Wang, J. Polleux, J. Lim, and B. Dunn, "Pseudocapacitive contributions to electrochemical energy storage in TiO_2 (anatase) nanoparticles," *Journal of Physical Chemistry C*, vol. 111, no. 40, pp. 14925–14931, 2007.

[36] M. Aguilar-Frutis, G. Reyna-Garcia, M. Garcia-Hipolito, J. Guzman-Mendoza, and C. Falcony, "Optical, structural, and electrical characteristics of high dielectric constant zirconium oxide thin films deposited by spray pyrolysis," *Journal of Vacuum Science and Technology A*, vol. 22, no. 4, pp. 1319–1325, 2004.

[37] M. Salavati-Niasari, M. Dadkhah, and F. Davar, "Pure cubic ZrO_2 nanoparticles by thermolysis of a new precursor," *Polyhedron*, vol. 28, no. 14, pp. 3005–3009, 2009.

[38] A. K. Singh, V. Viswanath, and V. C. Janu, "Synthesis, effect of capping agents, structural, optical and photoluminescence properties of ZnO nanoparticles," *Journal of Luminescence*, vol. 129, no. 8, pp. 874–878, 2009.